



1 **Impact of in-cloud aqueous processes on the chemical**
2 **compositions and morphology of individual atmospheric**
3 **aerosols**

4 Yuzhen Fu^{1,2}, Qin hao Lin^{1,#}, Guohua Zhang^{1,3*}, Yuxiang Yang^{1,2}, Yiping Yang^{2,4},
5 Xiufeng Lian^{1,2}, Long Peng^{1,2}, Feng Jiang^{1,2,##}, Xinhui Bi^{1,3*}, Lei Li⁵, Yuanyuan
6 Wang⁶, Duohong Chen⁷, Jie Ou⁸, Xinming Wang^{1,3}, Ping'an Peng^{1,3}, Jianxi Zhu³,
7 Guoying Sheng¹

8 ¹ State Key Laboratory of Organic Geochemistry and Guangdong Key Laboratory of Environmental
9 Protection and Resources Utilization, Guangzhou Institute of Geochemistry, Chinese Academy of
10 Sciences, Guangzhou 510640, PR China

11 ² University of Chinese Academy of Sciences, Beijing 100049, PR China

12 ³ Guangdong-Hong Kong-Macao Joint Laboratory for Environmental Pollution and Control, Guangzhou
13 510640, PR China

14 ⁴ CAS Key Laboratory of Mineralogy and Metallogeny & Guangdong Provincial Key Laboratory of
15 Mineral Physics and Materials, Guangzhou Institute of Geochemistry, CAS, Guangzhou 510640, PR
16 China

17 ⁵ Institute of Mass Spectrometer and Atmosphere Environment, Jinan University, Guangzhou 510632,
18 PR China

19 ⁶ Department of Atmospheric Science, School of Earth Science, Zhejiang University, Hangzhou 310027,
20 PR China

21 ⁷ State Environmental Protection Key Laboratory of Regional Air Quality Monitoring, Guangdong
22 Environmental Monitoring Center, Guangzhou 510308, PR China

23 ⁸ Shaoguan Environmental Monitoring Center, Shaoguan 512026, PR China

24 [#] now at: Guangdong Key Laboratory of Environmental Catalysis and Health Risk Control, Guangzhou
25 Key Laboratory Environmental Catalysis and Pollution Control, School of Environmental Science and
26 Engineering, Institute of Environmental Health and Pollution Control, Guangdong University of
27 Technology, Guangzhou 510006, PR China.

28 ^{##} now at: Institute of Meteorology and Climate Research, Karlsruhe Institute of Technology, Eggenstein-
29 Leopoldshafen 76344, Germany.

30 *Correspondence to: Guohua Zhang (zhanggh@gig.ac.cn) and Xinhui Bi (bixh@gig.ac.cn)



31 **Abstract.** The composition, morphology, and mixing structure of individual cloud residues (RES) and interstitial
32 particles (INT) at a mountain-top site were investigated. Eight types of particles were identified, including sulfate-
33 rich (S-rich), S-organic matter (OM), aged soot, aged mineral, aged fly ash, aged metal, fresh mixture, and aged
34 mixture. A shift of dominant particle types from S-rich (29%) and aged soot (27%) in the INT to S-OM (24%)
35 and aged mixture (22%) in the RES is observed. In particular, particles with organic shells are enriched in the
36 RES (30%) relative to the INT (12%). Our results highlight the in-cloud formation of more oxidized organic shells
37 on the activated particles. We also show that in-cloud processes may result in less compact soot, with the fractal
38 dimensions (D_f) of soot in the RES (1.82 ± 0.12) lower than those in the INT (2.11 ± 0.09). This research
39 emphasizes the role of in-cloud processes on the chemistry and microphysical properties of individual particles.
40 Given that organic coatings may determine the particle hygroscopicity, activation ability, and heterogeneous
41 chemical reactivity, the increase of OM-shelled particles upon in-cloud processes should have considerable
42 implications.



43 1 Introduction

44 Aerosol-cloud interaction is regarded as one of the most significant sources of uncertainty in assessing the
45 radiative forcing of aerosols so far (IPCC, 2013). On the one hand, aerosols can participate in the formation of
46 cloud droplets, which is primarily influenced by their chemical composition and size at a certain supersaturation
47 (Fan et al., 2016; Maskey et al., 2017; Ogawa et al., 2016; Raymond and Pandis, 2002; Zelenyuk et al., 2010). On
48 the other hand, in-cloud processes, including the formation of sulfate, nitrate, and water-soluble organics, and the
49 physical processes such as collision and coagulation, would substantially change the physical and chemical
50 properties of the activated particles (Kim et al., 2019; Ma et al., 2013; Roth et al., 2016; Wu et al., 2013). Given
51 that the morphology and mixing state are vital in determining the optical properties of particles (Adachi et al.,
52 2010; Wu et al., 2018), changes of these properties upon in-cloud processes would further affect the subsequent
53 atmospheric processes (e.g., cloud activation, heterogeneous reactions) and radiative forcing of particles after
54 droplet evaporation.

55 Understanding the morphology and mixing state of particles upon in-cloud processes is of considerable
56 significance to improve the knowledge of aerosol-cloud interactions. For instance, Zelenyuk et al. (2010) found
57 that both cloud droplet residues (RES) and interstitial particles (INT, or unactivated particles in the cloud) are
58 mainly composed of organics, sulfate, biomass burning particles, and processed sea salt at the North Slope of
59 Alaska. Kamphus et al. (2010) observed that 92% of RES are particles containing sulfates, organics, and nitric
60 oxide at the Jungfraujoch (Swiss Alps). At Mt. Tai, Liu et al. (2018b) observed that main particle types are S
61 (sulfate)-soot (36%), S-fly ash/metal-soot (26%) and S-rich (24%) for RES and S-rich (61%), S-soot (15%) and
62 soot (15%) for INT. These results indicate that both RES and INT present complex mixtures, generally
63 decomposed as mixing state between carbonaceous (i.e., organic materials (OM) and soot) and inorganic
64 compositions.

65 While there are extensive studies reporting the extent of aqueous phase processing on the modification of
66 aerosol bulk (e.g., mass) and/or chemical (e.g., mixing state, hygroscopicity) properties (Chakraborty et al., 2016;
67 Ervens et al., 2011), the influence of in-cloud processes on the physical properties (e.g., shape, mixing structure)
68 of individual particles is still ambiguous. In particular, physical properties can become dominant in the role of
69 cloud activation for particles with inorganic/organic mixed (Topping et al., 2007). A hydrophobic organic-rich
70 coating will form on a hygroscopic particle core if liquid-liquid phase separation occurs (Song et al., 2013).
71 Besides, the distribution of organics and its association with other aerosol types is also crucial for the correct
72 calculation of its radiative effects (Zhu et al., 2017). However, to what extent in-cloud processes play a role in
73 reshaping the distribution of organic and inorganic compositions remains unknown, although such coating
74 structures have been identified in ambient aerosols (Adachi and Buseck, 2008; Li and Shao, 2010; Yu et al., 2019).
75 Considering that in-cloud processes contribute to a substantial fraction (up to 60%) of organic aerosols (Ervens et
76 al., 2011; Liu et al., 2012; Myriokefalitakis et al., 2011; Spracklen et al., 2011), this process might not be neglected.

77 For another type of carbonaceous material, soot, there is extensive evidence that the absorption and cloud
78 activation of soot-containing particles can be significantly affected by coatings (Adachi et al., 2010; Wu et al.,



79 2018). The critical factors to accurately predicting of such impact include the amount and nature of the coating
80 material, the exact particle morphology, and the size distribution (Qiu et al., 2012; Radney et al., 2014). Fractal
81 dimension (D_f) is widely used to indicate the extent of branching of soot (Brasil et al., 1999), with densely packed
82 or compacted soot particles having higher D_f than chain-like branched clusters or open structures. While some
83 studies have found that soot compaction occurs after cloud processing (Bhandari et al., 2019; Ma et al., 2013;
84 Mikhailov et al., 2006), Khalizov et al. (2013) suggested that soot with thin organic coating did not become more
85 compact under high humidity. However, the morphology and mixing structure of soot involving the formation of
86 organics upon cloud processing is also poorly constrained because of the limited field observation.

87 To further improve our understanding of the morphology and mixing structures between the various
88 components within individual RES and INT, we conducted a 25-day field observation of cloud events at a
89 background site in southern China. A transmission electron microscope (TEM) combined with energy-dispersive
90 X-ray spectrometry (EDS) was used to analyze the chemical composition, size, morphology, and mixing structure
91 of individual RES and INT. Previously, the chemical composition and mixing state of RES at the same site have
92 been investigated with a single particle aerosol mass spectrometer (SPAMS) (Lin et al., 2017; Zhang et al., 2017a).
93 Herein, we focus on the mixing structure (e.g., chemical compositions and morphology) of individual particles,
94 in particular, OM-containing particles. Meanwhile, particle types and mixing state of RES and INT are also
95 discussed. The difference between the mixing structure of RES and INT may indicate the impact of in-cloud
96 aqueous processes.

97 **2 Materials and Methods**

98 **2.1 Sampling site**

99 Sampling was conducted at the top of Mt. Tianjing (112°53'56" E; 24°41'56" N; 1690 m above sea level) in
100 southern China from 18 May to 11 June 2017. The sampling site is located in a natural preserve, and it is almost
101 unaffected by local anthropogenic sources. It is about 50 km and 350 km away from the north of the Pearl River
102 Delta (PRD) region and the South China Sea, respectively.

103 **2.2 Collection of RES and INT**

104 A cloud event was identified with visibility below a threshold of 3 km and relative humidity (RH) above a
105 threshold of 95%, using a ground-based counterflow virtual impactor (GCVI, model 1205, Brechtel Mfg. Inc.,
106 USA). The GCVI was automatically triggered when there was a cloud event, whereas it was not allowed to sample
107 when a precipitation sensor detected rain or snow. Then cloud droplets were introduced into the GCVI, followed
108 by removing water in an evaporation chamber (40 °C) to obtain RES. The sampling process might experience
109 some particle loss due to the evaporation of highly volatile substances. The droplet cut size, at which the
110 transmission efficiency of CVI was 50%, was set at a size larger than 7.5 μm (Shingler et al., 2012). INT was
111 sampled using another inlet (PM_{2.5} cyclone inlet, 5 lpm), followed by passing through a silica gel diffusion dryer.

112 A DKL-2 sampler (Genstar Electronic Technology Co., Ltd., China) was used to collect RES and INT on copper
113 grids coated with carbon film with an airflow of 1 L min⁻¹. The collection efficiency of the sampler is 50% at 80



114 nm, assuming the particle density is 2 g cm^{-3} . To avoid particle overlapping, the sampling duration was set within
115 10 minutes. All samples were placed in a sealed plastic sample box and stored in a desiccator at room temperature
116 for subsequent analysis.

117 The information about cloud events and samples are summarized in Table S1. We focused on three cloud events
118 (#1, #2, and #3), with a duration of 14, 34, and 47 hours, respectively. RES and INT samples from these cloud
119 events were analyzed, with INT not available for the cloud event #1. To minimize the influence of rapid change
120 of cloud condition, all the samples were collected during the stable and mature periods (Visibility $< 100 \text{ m}$).

121 2.3 Analysis of RES and INT

122 Chemical composition, size, and morphology of individual RES and INT were characterized by a TEM (FEI
123 Talos F200S) operated at 200 kV. TEM/EDS is a very effective tool to analyze the microscopic characteristics of
124 individual particles. The resolution of images between $1 \mu\text{m}$ and 100 nm can be magnified from 7,000 to 36,000
125 folds, which depended on the size of particles. The EDS is coupled with TEM to detect the intensity of elements
126 heavier than carbon ($Z \geq 6$). The produced X-rays signal in the EDS system is detected by a silicon (Si) drift
127 detector (SSD), and thus Si is not considered in the discussion. Cu is also not considered due to the interference
128 from the copper grids. In the TEM vacuum chamber, some volatile substances (e.g., NH_4NO_3 and volatile
129 organic matter) would be lost. Moreover, volatile materials are often sensitive to strong electron beams. Due to
130 the analysis error of volatile materials, TEM/EDS studies typically focus on refractory compositions. Using an
131 image analysis software (ImageJ), the equivalent circle diameters (ECD) of all particles can be obtained from the
132 scanned images from the TEM. For particles with rim, only the nucleus is counted, because the rims contain only
133 a small amount of OM. Overall, 780 particles, including RES and INT, were analyzed. A SPAMS (Hexin
134 Analytical Instrument Co., Ltd., Guangzhou, China) was used to analyse the chemical composition of RES and
135 INT simultaneously in real-time, and the data of SPAMS is not the focus of this study.

136 2.4 Calculating morphology parameters of soot

137 The fractal dimension of soot is characterized in the following statistical scaling law (Brasil et al., 1999; Köylü
138 et al., 1995):

$$139 \quad N = k_g \left(\frac{2R_g}{d_p} \right)^{D_f}$$

140 Where N is the number of monomers within a certain soot aggregate, k_g is the fractal pre-factor, R_g is the radius
141 of gyration, d_p is the diameter of the monomer, and D_f is the mass fractal dimension. R_g can be obtained by using
142 a simple relationship between R_g and L_{max} , the maximum length of the soot aggregate (Brasil et al., 1999):

$$143 \quad L_{max}/2R_g = 1.50 \pm 0.05$$

144 And, the number of monomers, N , can be calculated by a power-law correlation of projected area of monomer
145 and aggregate:



146
$$N = k_a \left(\frac{A_a}{A_p} \right)^\alpha$$

147 Where k_a is a constant, A_a and A_p are the projected area of aggregate and monomer, respectively, and α is an
148 empirical projected area exponent. The value of k_a and α depends on the degree of monomer overlap in the
149 aggregate. The detailed calculation process has been described elsewhere (Wang et al., 2017).

150 3 Results and Discussion

151 3.1 Particle type and mixing state of RES and INT

152 According to mixing state, RES and INT were divided into following eight types (Figure 1): S-rich, S-OM,
153 fresh mixture (soot/mineral/metal/fly ash), aged soot (S/OM-soot), aged mineral (S/OM-mineral), aged metal
154 (S/OM-metal), aged fly ash (S/OM-fly ash), and aged mixture (S/OM-soot/mineral/metal/fly ash). The details
155 involving the identification of each component (S, OM, soot, mineral, metal, fly ash) are provided in the
156 Supporting Information. S-rich or OM, generally considered to be aged since they are mainly secondarily
157 produced in the atmosphere, are internally mixed with refractory fractions (soot/mineral/metal/fly ash)
158 (Canagaratna et al., 2007; Huang et al., 2012; Jiang et al., 2019). Such internally mixed S/OM-refractory particles
159 are named as aged refractory particles herein. Particle types containing two or more refractory components are
160 named as “mixture”. It is worth noting that fresh mixture are refractory particles without S-rich and OM, which
161 are collectively defined as the fresh mixture due to the small amount.

162 Figure 2 shows the number fraction of different particle types in the RES and INT during cloud events #2 and
163 #3. S-rich, S-OM, aged soot, and aged mixture particles are dominant particle types. The most abundant particles
164 in the RES are aged mixture (23%), followed by S-OM (22%), aged soot (20%), S-rich (16%), aged metal (9%),
165 aged fly ash (5%), aged mineral (4%), and fresh mixture (1%). Differently, INT is predominated by S-rich (29%),
166 aged soot (27%), S-OM (15%), aged mixture (10%), and the lesser percentage of aged fly ash (8%), fresh mixture
167 (5%), aged mineral (4%), and aged metal (2%) were also observed. Among three cloud events, the RES are
168 dominated by S-OM in cloud event #1 and #2 and aged mixture particles in cloud event #3 (Figure S1). Influenced
169 by air masses (Figure S1, S2), the proportion of aged mineral particles in the RES during cloud event #1 (14%) is
170 nearly four times those in the other two cloud events. Aged fly ash particles have the highest proportion in cloud
171 event #3 (10%) compared with the other two cloud events. However, the influence of air masses on the
172 compositions of the RES during cloud events #2 and #3 is limited, as confirmed by the SPAMS data (Figure S4).
173 It is also shown that the RES and INT analyzed by TEM/EDS can represent their compositions throughout cloud
174 events #2 and #3, since such compositions were relatively stable throughout these periods (Figure S5).

175 3.2 The morphology and mixing structure of carbonaceous particles

176 OM-containing particles, including all the S-OM particles, part of aged refractory (S-OM/OM-refractory), and
177 aged mixture (S-OM/OM-soot/mineral/metal/fly ash) particles, accounted for 60% of RES and 33% of INT during
178 cloud events #2 and #3. According to the mixing structures between OM and other materials (Figure 3), OM-
179 containing particles are classified into the following five categories: coating (Figure 3b), core-shell (Figure 3c),



180 embedded (Figure 3d), attached (Figure 3e) and homogenous-like (Figure 3f) structures (Li et al., 2016). A particle
181 is classified as coating structure when wrapped with a thin layer of OM. The thickness of the coating layer ranges
182 from 12 to 150 nm. Generally, the shapes of OM-containing particles with coating structure are elliptical or
183 irregular. The difference between the core-shell structure and coating structure is the relative thickness of OM:
184 Core-shell structure possessed thicker organics than coating structure. The thickness of the shell varies from 86
185 to 2110 nm, and the ratio of the projected area of the shell to particle ranges from 0.20 to 0.97. Moreover, OM-
186 containing particles with core-shell structure are round. Embedded structure refers to the particle with OM
187 embedded in other materials (e.g., sulfate). The attached structure refers to the particle of OM attached to other
188 materials. The homogenous-like structure represents particles with evenly mixed and no identifiable boundary
189 between organic and non-organic matter.

190 The first most abundant particles are coating geometry comprising 53% of RES and 59% of INT during cloud
191 event #2 and #3, respectively. The second are core-shell particles for RES and attached particles for INT. The
192 percentage of core-shell particles in the RES is almost 2.5 times that in the INT (27% vs. 12%). Embedded and
193 homogenous-like particles account for minor proportions (< 4%) for both RES and INT.

194 Soot-containing particles, including all the aged soot particles (S/OM-soot) and part of a fresh mixture
195 (soot/mineral/metal/fly ash) and aged mixture particles (S/OM-soot/mineral/metal/fly ash), account for 36% of
196 RES and 39% of INT during cloud event #2 and #3, respectively. The fraction is consistent with the range of those
197 (< 30% – ~60%) observed at the same site by SPAMS (Zhang et al., 2017a). Most of the soot are distributed
198 around the periphery of particles (Figure S6). Figure 4 shows the D_f of soot within RES and INT of cloud event
199 #2 and #3. The result shows that the D_f of soot is smaller in the RES (1.82 ± 0.12) than in the INT (2.11 ± 0.09),
200 which means that soot is more branched in the RES. It is noted that 62.5% of all soot-containing particles with
201 clear boundaries are included in the D_f calculation since thick coating around soot might make the boundary of
202 monomers not clear enough (Bhandari et al., 2019). The obtained D_f are close to those (1.83 – 2.16) reported at a
203 background site (Wang et al., 2017). The D_f of soot in the RES and INT likely represents partly coated soot (1.82
204 ± 0.05) (Yuan et al., 2019) and embedded soot (2.16 ± 0.05) (Wang et al., 2017), respectively. In addition to
205 emission sources and coating processes, high relative humidity (RH) during nighttime is a critical factor to
206 increase the compactness of soot (Yuan et al., 2019).

207 3.3 In-cloud formation of OM

208 It can be seen from Figure 2 that a shift of dominant particle types from S-rich (29%) and aged soot (27%) in
209 the INT to the aged mixture (23%) and S-OM (22%) in the RES. In particular, the fraction of OM-containing
210 particles increases from 33% in the INT to 60% in the RES. It is unlikely due to the favorable activation of S-OM
211 or aged mixture, since mixing with OM generally lower the hygroscopicity of inorganic-dominant particles (e.g.,
212 S-rich) (Brooks et al., 2004; Pierce et al., 2012). OM coating at the same site has been shown to inhibit the CCN
213 activation of soot-containing particles (Zhang et al., 2017a). Instead, it is most probably attributed to the in-cloud
214 formation of OM on the surface of some S-rich particles, shifting the dominant particle type from S-rich to S-OM
215 particles. It can be supported by the relatively larger median size of S-OM particles ($0.76 \mu\text{m}$) than S-rich particles
216 ($0.56 \mu\text{m}$) (Figure S7), since in-cloud formation of OM is expected to enlarge the original S-rich particles (Pierce
217 et al., 2012).



218 In addition, the fraction of OM-containing particles with core-shell mixing structure in the RES is almost 2.5
219 times that in the INT (Figure 3a). Such a mixing structure is similar to those observed in the Arctic, background,
220 or rural atmosphere (Hiranuma et al., 2013; Li et al., 2016; Yu et al., 2019), but is different from previous findings
221 in polluted air where OM is typically mixed with sulfate (Li et al., 2016). It is also consistent with several
222 laboratory simulations demonstrating that reactive uptake of volatile organic compounds (VOCs) on inorganic
223 sulfate and follow-up strong interactions between these species would lead to a core-shell morphology (e.g., Zhang
224 et al., 2018; Riva et al., 2019; Zhang et al., 2019). Our results support the hypothesis that the core-shell morphology
225 with secondary organic aerosol (SOA) in the shell phase is predominant (Gorkowski et al., 2020). Based on the
226 measurements from aerosol optical tweezers experiments and literature data, the authors come up with a particle
227 morphology prediction framework developed for mixtures of organic aerosol.

228 Moreover, we estimated the O/C ratio of coating and shell within OM-containing particles. It should be noted
229 that the O/C ratio of organic coating and shell is underestimated herein due to the copper grid evenly covered by
230 carbon film. Nevertheless, the average value of the O/C ratio of RES is higher than INT, and the average value of
231 the O/C ratio of RES with core-shell structure is two times that with coating structure (Table S2), indicating that
232 these RES with core-shell particles are more oxidized. At the same site, we have previously observed enhanced
233 aqueous SOA, such as oxalate in the cloud (Zhang et al., 2017b). Higher O/C ratio of core-shell particles is also
234 consistent with current studies reporting more oxidized organic species in cloud/fog residues (Brege et al., 2018;
235 Chakraborty et al., 2016; Zhang et al., 2017b). With high levels of VOCs at the sampling site (Lv et al., 2019),
236 prevalent formation of aqueous SOA through the uptake of VOCs in cloud droplets would be expected (Kim et
237 al., 2019; Liu et al., 2018a). The contribution from photochemical processes may also be reflected by the
238 association of the highest fraction (81%) of OM-containing particles with a higher concentration of O₃ during
239 cloud event #2 (Table S3).

240 However, one may expect that such core-shell mixing structure in the RES can also be explained by the primary
241 activation of S-OM particles with larger sizes. Unfortunately, no sample is available before cloud events. However,
242 with evidence from the collocated SPAMS, we show that this is not convincing. As shown in Table S4, the ratios
243 of relative peak area between organics and sulfate are similar between the INT and particles before cloud event,
244 whereas they are higher in the RES. This is corresponding to the production of oxidized organics during in-cloud
245 processes (Zhang et al., 2017b). It is noted that while some loss of volatile organic compounds during the
246 TEM/EDS analysis may affect the O/C of particles, the relatively higher O/C ratio for the RES is still affirmative.
247 Droplets are expected to dissolve more abundance of volatile organic compounds (Chakraborty et al., 2016),
248 evaporation of which would result in an underestimate of O/C to a higher degree rather than the INT.

249 3.4 The D_f of soot in the RES and INT

250 While some previous studies demonstrated that soot aggregates tend to be more compact (with larger D_f) after
251 aging or cloud processing (Adachi and Buseck, 2013; Wu et al., 2018), our results suggest that in-cloud processes
252 may result in more branched soot, as shown in Figure 4. Considering that D_f is controlled mainly by emission
253 sources, combustion conditions, and aging processes (Adachi et al., 2007), we propose three possible explanations
254 for the lower D_f of soot in the RES than that in the INT. The first and the most likely reason is that the relatively
255 large deformation and reconfiguration of soot aggregates are inhibited when non-volatile materials fill the spaces



256 between the branches during transport and activation into cloud droplets (Zhang et al., 2018). And, if the soot
257 aggregates are not coated by non-volatile materials, they may shrink and become more compact during long-
258 distance transport (Adachi and Buseck, 2013). We show that soot aggregates in the INT have higher D_f and lower
259 average ECD (247 nm vs. 266 nm) than that in the RES, which means that smaller, tighter soot particles are less
260 likely to act as CCN, and larger, less dense soot particles are likely to act as CCN. This is consistent with a study
261 reporting that small particles are more compact than large particles (Adachi et al., 2014). The second is that water-
262 soluble substances within aerosols will be miscible after activating to cloud droplets (Gorkowski et al., 2020), and
263 the coating materials of soot may be released, which makes soot more branched in the droplets and the following-
264 up droplet evaporation. The third possible explanation is that different combustion materials and combustion
265 conditions produce soot-containing particles with different mixing states and morphology (China et al., 2014;
266 Khalizov et al., 2013; Liu et al., 2017; Zhang et al., 2018).

267 This result is in contrast to the current study reporting that soot sampled after cloud droplet evaporating are
268 more compact than freshly emitted and interstitial soot (Bhandari et al., 2019). Our observations in the background
269 site show that the majority of soot aggregates in both RES and INT (~80%) are located in off-center positions,
270 having less compact shapes even after being coated. This is quite different from the core-shell model currently
271 used in the climate models (Bond and Bergstrom, 2006; Wu et al., 2018). Through theoretical calculation, Adachi
272 et al. (2010) suggested that absorption cross-sections could be reduced by 20-30% with off-center positions of
273 soot relative to center positions. This means that the models based on core-shell assumption may overestimate the
274 absorption of soot-containing particles after cloud processing.

275 **4 Conclusion and atmospheric implications**

276 The result highlights the different morphology and mixing structures of activated and interstitial particles,
277 which may imply the substantial role of in-cloud aqueous processes in reshaping the activated particles. While Yu
278 et al. (2019) considered organic coatings on sulfate in the Arctic as a result of the increase of SOA following
279 particle aging and growth during transport, our data further imply a specific role of in-cloud processes in the
280 coating on sulfate. The prevalence of OM shelled particles upon in-cloud processes also supports a recent
281 laboratory observation depicting that rapid film formation and fast heterogeneous oxidation can provide an
282 efficient way of converting water-insoluble organic films into more water-soluble components in aerosols or cloud
283 droplets (Aumann and Tabazadeh, 2008).

284 Gorkowski et al. (2020) suggested that mixing structures of OM-containing particles are related to the oxidation
285 degree of OM. We also show that OM shells formed in-cloud have a higher degree of oxidation. Such a chemical
286 and morphology modification of aerosol particles may influence species diffusivities from the interior to the
287 surface region of the shell and gas-particle partitioning between the shell and gas (Liu et al., 2016; Shiraiwa et al.,
288 2013). Such a reshaping may also have an influence on aerosol hygroscopicity. Extrapolating the linear
289 relationship between the O/C ratio and the hygroscopicity parameter (κ_{org}) indicates that $\kappa_{\text{org-shell}}$ is about 1.4 times
290 $\kappa_{\text{org-coating}}$ (Jimenez et al., 2009; Lambe et al., 2011). In addition, the formation of the organic film could result in
291 a change of surface tension and thus affect the critical supersaturation required for particle activation (Ovadnevaite
292 et al., 2017). For mineral particles, the heterogeneous ice nucleation potential may be suppressed when coated by



293 OM (Möhler et al., 2008). Given the critical contribution of in-cloud aqueous SOA, several mixing structures of
294 OM-containing aerosols upon in-cloud processes may have substantial implications in modeling the direct and
295 indirect radiative forcing of aerosols (Scott et al., 2014; Zhu et al., 2017).

296

297 *Data availability.* Data are available on request from Guohua Zhang (zhanggh@gig.ac.cn) and Xinhui Bi
298 (bixh@gig.ac.cn).

299 *Author contribution.* GHZ and XHB designed the research (with input from XMW and GYS). YZF, GHZ, and
300 XHB analyzed the data, and wrote the manuscript. YZF, XFL, YXY, FJ, and QHL conducted sampling work
301 under the guidance of GHZ, XHB and XMW. LL, DHC and JO had an active role in supporting the sampling
302 work. YZF performed the laboratory analysis of individual particles by TEM/EDS, with support from YPY and
303 JXZ. All authors contributed to the discussions of the results and refinement of the manuscript.

304 *Competing interests.* The authors declare that they have no conflict of interest.

305 *Acknowledgements.* This work was supported by the National Nature Science Foundation of China (No. 41775124
306 and 41877307), Natural Science Foundation of Guangdong Province (2019B151502022), and Guangdong
307 Foundation for Program of Science and Technology Research (Grant No. 2019B121205006 and
308 2017B030314057). The authors gratefully acknowledge the NOAA Air Resources Laboratory (ARL) for the
309 provision of the HYSPLIT transport and dispersion model (<http://ready.arl.noaa.gov>) used in this publication.

310 References

- 311 Adachi, K., Chung, S. H., Friedrich, H., and Buseck, P. R.: Fractal parameters of individual soot particles
312 determined using electron tomography: Implications for optical properties, *Journal of Geophysical Research-*
313 *Atmospheres*, 112, D14202, 10.1029/2006jd008296, 2007.
- 314 Adachi, K., and Buseck, P. R.: Internally mixed soot, sulfates, and organic matter in aerosol particles from Mexico
315 City, *Atmospheric Chemistry and Physics*, 8, 6469-6481, 10.5194/acp-8-6469-2008, 2008.
- 316 Adachi, K., Chung, S. H., and Buseck, P. R.: Shapes of soot aerosol particles and implications for their effects on
317 climate, *Journal of Geophysical Research-Atmospheres*, 115, D15206, 10.1029/2009jd012868, 2010.
- 318 Adachi, K., and Buseck, P. R.: Changes of ns-soot mixing states and shapes in an urban area during CalNex,
319 *Journal of Geophysical Research-Atmospheres*, 118, 3723-3730, 10.1002/jgrd.50321, 2013.
- 320 Adachi, K., Zaizen, Y., Kajino, M., and Igarashi, Y.: Mixing state of regionally transported soot particles and the
321 coating effect on their size and shape at a mountain site in Japan, *Journal of Geophysical Research-Atmospheres*,
322 119, 5386-5396, 10.1002/2013jd020880, 2014.
- 323 Aumann, E., and Tabazadeh, A.: Rate of organic film formation and oxidation on aqueous drops, *Journal of*
324 *Geophysical Research-Atmospheres*, 113, D23205, 10.1029/2007jd009738, 2008.
- 325 Bhandari, J., China, S., Chandrakar, K. K., Kinney, G., Cantrell, W., Shaw, R. A., Mazzoleni, L. R., Giroto, G.,
326 Sharma, N., Gorkowski, K., Gilardoni, S., Decesari, S., Facchini, M. C., Zanca, N., Pavese, G., Esposito, F.,
327 Dubey, M. K., Aiken, A. C., Chakrabarty, R. K., Moosmüller, H., Onasch, T. B., Zaveri, R. A., Scarnato, B.



- 328 V., Fialho, P., and Mazzoleni, C.: Extensive Soot Compaction by Cloud Processing from Laboratory and Field
329 Observations, *Scientific reports*, 9, 11824-11824, 10.1038/s41598-019-48143-y, 2019.
- 330 Bond, T. C., and Bergstrom, R. W.: Light absorption by carbonaceous particles: An investigative review, *Aerosol*
331 *Science and Technology*, 40, 27-67, 10.1080/02786820500421521, 2006.
- 332 Brasil, A. M., Farias, T. L., and Carvalho, M. G.: A recipe for image characterization of fractal-like aggregates,
333 *Journal of Aerosol Science*, 30, 1379-1389, 10.1016/s0021-8502(99)00026-9, 1999.
- 334 Brege, M., Paglione, M., Gilardoni, S., Decesari, S., Facchini, M. C., and Mazzoleni, L. R.: Molecular insights on
335 aging and aqueous-phase processing from ambient biomass burning emissions-influenced Po Valley fog and
336 aerosol, *Atmospheric Chemistry and Physics*, 18, 13197-13214, 10.5194/acp-18-13197-2018, 2018.
- 337 Brooks, S. D., DeMott, P. J., and Kreidenweis, S. M.: Water uptake by particles containing humic materials and
338 mixtures of humic materials with ammonium sulfate, *Atmospheric Environment*, 38, 1859-1868,
339 10.1016/j.atmosenv.2004.01.009, 2004.
- 340 Canagaratna, M. R., Jayne, J. T., Jimenez, J. L., Allan, J. D., Alfarra, M. R., Zhang, Q., Onasch, T. B., Drewnick,
341 F., Coe, H., Middlebrook, A., Delia, A., Williams, L. R., Trimborn, A. M., Northway, M. J., DeCarlo, P. F.,
342 Kolb, C. E., Davidovits, P., and Worsnop, D. R.: Chemical and microphysical characterization of ambient
343 aerosols with the aerodyne aerosol mass spectrometer, *Mass Spectrometry Reviews*, 26, 185-222,
344 10.1002/mas.20115, 2007.
- 345 Chakraborty, A., Ervens, B., Gupta, T., and Tripathi, S. N.: Characterization of organic residues of size-resolved
346 fog droplets and their atmospheric implications, *Journal of Geophysical Research-Atmospheres*, 121, 4317-
347 4332, 10.1002/2015jd024508, 2016.
- 348 China, S., Salvadori, N., and Mazzoleni, C.: Effect of Traffic and Driving Characteristics on Morphology of
349 Atmospheric Soot Particles at Freeway On-Ramps, *Environmental Science & Technology*, 48, 3128-3135,
350 10.1021/es405178n, 2014.
- 351 Ervens, B., Turpin, B. J., and Weber, R. J.: Secondary organic aerosol formation in cloud droplets and aqueous
352 particles (aqSOA): a review of laboratory, field and model studies, *Atmospheric Chemistry and Physics*, 11,
353 11069-11102, 10.5194/acp-11-11069-2011, 2011.
- 354 Ervens, B., Sorooshian, A., Aldhaif, A. M., Shingler, T., Crosbie, E., Ziemba, L., Campuzano-Jost, P., Jimenez,
355 J. L., and Wisthaler, A.: Is there an aerosol signature of chemical cloud processing?, *Atmospheric Chemistry*
356 *and Physics*, 18, 16099-16119, 10.5194/acp-18-16099-2018, 2018.
- 357 Fan, J., Wang, Y., Rosenfeld, D., and Liu, X.: Review of Aerosol-Cloud Interactions: Mechanisms, Significance,
358 and Challenges, *Journal of the Atmospheric Sciences*, 73, 4221-4252, 10.1175/jas-d-16-0037.1, 2016.
- 359 Gorkowski, K., Donahue, N. M., and Sullivan, R. C.: Aerosol Optical Tweezers Constrain the Morphology
360 Evolution of Liquid-Liquid Phase-Separated Atmospheric Particles, *Chem*, 6, 204-220,
361 10.1016/j.chempr.2019.10.018, 2020.
- 362 Hiranuma, N., Brooks, S. D., Moffet, R. C., Glen, A., Laskin, A., Gilles, M. K., Liu, P., Macdonald, A. M., Strapp,
363 J. W., and McFarquhar, G. M.: Chemical characterization of individual particles and residuals of cloud droplets
364 and ice crystals collected on board research aircraft in the ISDAC 2008 study, *Journal of Geophysical Research-*
365 *Atmospheres*, 118, 6564-6579, 10.1002/jgrd.50484, 2013.



- 366 Huang, H., Ho, K. F., Lee, S. C., Tsang, P. K., Ho, S. S. H., Zou, C. W., Zou, S. C., Cao, J. J., and Xu, H. M.:
367 Characteristics of carbonaceous aerosol in PM_{2.5}: Pearl Delta River Region, China, *Atmospheric Research*,
368 104, 227-236, 10.1016/j.atmosres.2011.10.016, 2012.
- 369 Intergovernmental Panel on Climate Change (IPCC) (2013), *Climate Change 2013: the physical science basis*,
370 Cambridge University Press, Cambridge, United Kingdom and New York, NY, USA, 2013
- 371 Jiang, F., Liu, F., Lin, Q., Fu, Y., Yang, Y., Peng, L., Lian, X., Zhang, G., Bi, X., Wang, X., and Sheng, G.:
372 Characteristics and Formation Mechanisms of Sulfate and Nitrate in Size-segregated Atmospheric Particles
373 from Urban Guangzhou, China, *Aerosol and Air Quality Research*, 19, 1284-1293, 10.4209/aaqr.2018.07.0251,
374 2019.
- 375 Jimenez, J. L., Canagaratna, M. R., Donahue, N. M., Prevot, A. S. H., Zhang, Q., Kroll, J. H., DeCarlo, P. F.,
376 Allan, J. D., Coe, H., Ng, N. L., Aiken, A. C., Docherty, K. S., Ulbrich, I. M., Grieshop, A. P., Robinson, A.
377 L., Duplissy, J., Smith, J. D., Wilson, K. R., Lanz, V. A., Hueglin, C., Sun, Y. L., Tian, J., Laaksonen, A.,
378 Raatikainen, T., Rautiainen, J., Vaattovaara, P., Ehn, M., Kulmala, M., Tomlinson, J. M., Collins, D. R.,
379 Cubison, M. J., Dunlea, E. J., Huffman, J. A., Onasch, T. B., Alfarra, M. R., Williams, P. I., Bower, K., Kondo,
380 Y., Schneider, J., Drewnick, F., Borrmann, S., Weimer, S., Demerjian, K., Salcedo, D., Cottrell, L., Griffin, R.,
381 Takami, A., Miyoshi, T., Hatakeyama, S., Shimono, A., Sun, J. Y., Zhang, Y. M., Dzepina, K., Kimmel, J. R.,
382 Sueper, D., Jayne, J. T., Herndon, S. C., Trimborn, A. M., Williams, L. R., Wood, E. C., Middlebrook, A. M.,
383 Kolb, C. E., Baltensperger, U., and Worsnop, D. R.: Evolution of Organic Aerosols in the Atmosphere, *Science*,
384 326, 1525-1529, 10.1126/science.1180353, 2009.
- 385 Kamphus, M., Ettner-Mahl, M., Klimach, T., Drewnick, F., Keller, L., Cziczo, D. J., Mertes, S., Borrmann, S.,
386 and Curtius, J.: Chemical composition of ambient aerosol, ice residues and cloud droplet residues in mixed-
387 phase clouds: single particle analysis during the Cloud and Aerosol Characterization Experiment (CLACE 6),
388 *Atmospheric Chemistry and Physics*, 10, 8077-8095, 10.5194/acp-10-8077-2010, 2010.
- 389 Khalizov, A. F., Lin, Y., Qiu, C., Guo, S., Collins, D., and Zhang, R.: Role of OH-Initiated Oxidation of Isoprene
390 in Aging of Combustion Soot, *Environmental Science & Technology*, 47, 2254-2263, 10.1021/es3045339,
391 2013.
- 392 Kim, H., Collier, S., Ge, X., Xu, J., Sun, Y., Jiang, W., Wang, Y., Herckes, P., and Zhang, Q.: Chemical processing
393 of water-soluble species and formation of secondary organic aerosol in fogs, *Atmospheric Environment*, 200,
394 158-166, 10.1016/j.atmosenv.2018.11.062, 2019.
- 395 Köylü, Ü. Ö., Xing, Y. C., and Rosner, D. E.: Fractal morphology analysis of combustion-generated aggregates
396 using angular light scattering and electron microscope images, *Langmuir*, 11, 4848-4854, 10.1021/la00012a043,
397 1995.
- 398 Lambe, A. T., Onasch, T. B., Massoli, P., Croasdale, D. R., Wright, J. P., Ahern, A. T., Williams, L. R., Worsnop,
399 D. R., Brune, W. H., and Davidovits, P.: Laboratory studies of the chemical composition and cloud
400 condensation nuclei (CCN) activity of secondary organic aerosol (SOA) and oxidized primary organic aerosol
401 (OPOA), *Atmospheric Chemistry and Physics*, 11, 8913-8928, 10.5194/acp-11-8913-2011, 2011.
- 402 Li, W., and Shao, L.: Mixing and water-soluble characteristics of particulate organic compounds in individual
403 urban aerosol particles, *Journal of Geophysical Research-Atmospheres*, 115, D02301, 10.1029/2009jd012575,
404 2010.



- 405 Li, W., Sun, J., Xu, L., Shi, Z., Riemer, N., Sun, Y., Fu, P., Zhang, J., Lin, Y., Wang, X., Shao, L., Chen, J., Zhang,
406 X., Wang, Z., and Wang, W.: A conceptual framework for mixing structures in individual aerosol particles,
407 *Journal of Geophysical Research-Atmospheres*, 121, 13784-13798, 10.1002/2016jd025252, 2016.
- 408 Lin, Q., Zhang, G., Peng, L., Bi, X., Wang, X., Brechtel, F. J., Li, M., Chen, D., Peng, P. a., Sheng, G., and Zhou,
409 Z.: In situ chemical composition measurement of individual cloud residue particles at a mountain site, southern
410 China, *Atmospheric Chemistry and Physics*, 17, 8473-8488, 10.5194/acp-17-8473-2017, 2017.
- 411 Liu, F., Bi, X., Zhang, G., Lian, X., Fu, Y., Yang, Y., Lin, Q., Jiang, F., Wang, X., Peng, P., and Sheng, G.: Gas-
412 to-particle partitioning of atmospheric amines observed at a mountain site in southern China, *Atmospheric*
413 *Environment*, 195, 1-11, 10.1016/j.atmosenv.2018.09.038, 2018a.
- 414 Liu, J., Horowitz, L. W., Fan, S., Carlton, A. G., and Levy, H., II: Global in-cloud production of secondary organic
415 aerosols: Implementation of a detailed chemical mechanism in the GFDL atmospheric model AM3, *Journal of*
416 *Geophysical Research-Atmospheres*, 117, D15303, 10.1029/2012jd017838, 2012.
- 417 Liu, L., Kong, S., Zhang, Y., Wang, Y., Xu, L., Yan, Q., Lingaswamy, A. P., Shi, Z., Lv, S., Niu, H., Shao, L.,
418 Hu, M., Zhang, D., Chen, J., Zhang, X., and Li, W.: Morphology, composition, and mixing state of primary
419 particles from combustion sources - crop residue, wood, and solid waste, *Scientific Reports*, 7, 5047,
420 10.1038/s41598-017-05357-2, 2017.
- 421 Liu, L., Zhang, J., Xu, L., Yuan, Q., Huang, D., Chen, J., Shi, Z., Sun, Y., Fu, P., Wang, Z., Zhang, D., and Li,
422 W.: Cloud scavenging of anthropogenic refractory particles at a mountain site in North China, *Atmospheric*
423 *Chemistry and Physics*, 18, 14681-14693, 10.5194/acp-18-14681-2018, 2018b.
- 424 Liu, P., Li, Y. J., Wang, Y., Gilles, M. K., Zaveri, R. A., Bertram, A. K., and Martin, S. T.: Lability of secondary
425 organic particulate matter, *Proceedings of the National Academy of Sciences of the United States of America*,
426 113, 12643-12648, 10.1073/pnas.1603138113, 2016.
- 427 Lv, S., Gong, D., Ding, Y., Lin, Y., Wang, H., Ding, H., Wu, G., He, C., Zhou, L., Liu, S., Ristovski, Z., Chen,
428 D., Shao, M., Zhang, Y., and Wang, B.: Elevated levels of glyoxal and methylglyoxal at a remote mountain site
429 in southern China: Prompt in-situ formation combined with strong regional transport, *The Science of the total*
430 *environment*, 672, 869-882, 10.1016/j.scitotenv.2019.04.020, 2019.
- 431 Ma, X., Zangmeister, C. D., Gigault, J., Mulholland, G. W., and Zachariah, M. R.: Soot aggregate restructuring
432 during water processing, *Journal of Aerosol Science*, 66, 209-219, 10.1016/j.jaerosci.2013.08.001, 2013.
- 433 Maskey, S., Chong, K. Y., Seo, A., Park, M., Lee, K., and Park, K.: Cloud Condensation Nuclei Activation of
434 Internally Mixed Black Carbon Particles, *Aerosol and Air Quality Research*, 17, 867-877,
435 10.4209/aaqr.2016.06.0229, 2017.
- 436 Mikhailov, E. F., Vlasenko, S. S., Podgorny, I. A., Ramanathan, V., and Corrigan, C. E.: Optical properties of
437 soot-water drop agglomerates: An experimental study, *Journal of Geophysical Research-Atmospheres*, 111,
438 D07209, 10.1029/2005jd006389, 2006.
- 439 Möhler, O., Benz, S., Saathoff, H., Schnaiter, M., Wagner, R., Schneider, J., Walter, S., Ebert, V., and Wagner,
440 S.: The effect of organic coating on the heterogeneous ice nucleation efficiency of mineral dust aerosols,
441 *Environmental Research Letters*, 3, 025007, 10.1088/1748-9326/3/2/025007, 2008.
- 442 Myriokefalitakis, S., Tsigaridis, K., Mihalopoulos, N., Sciare, J., Nenes, A., Kawamura, K., Segers, A., and
443 Kanakidou, M.: In-cloud oxalate formation in the global troposphere: a 3-D modeling study, *Atmospheric*
444 *Chemistry and Physics*, 11, 5761-5782, 10.5194/acp-11-5761-2011, 2011.



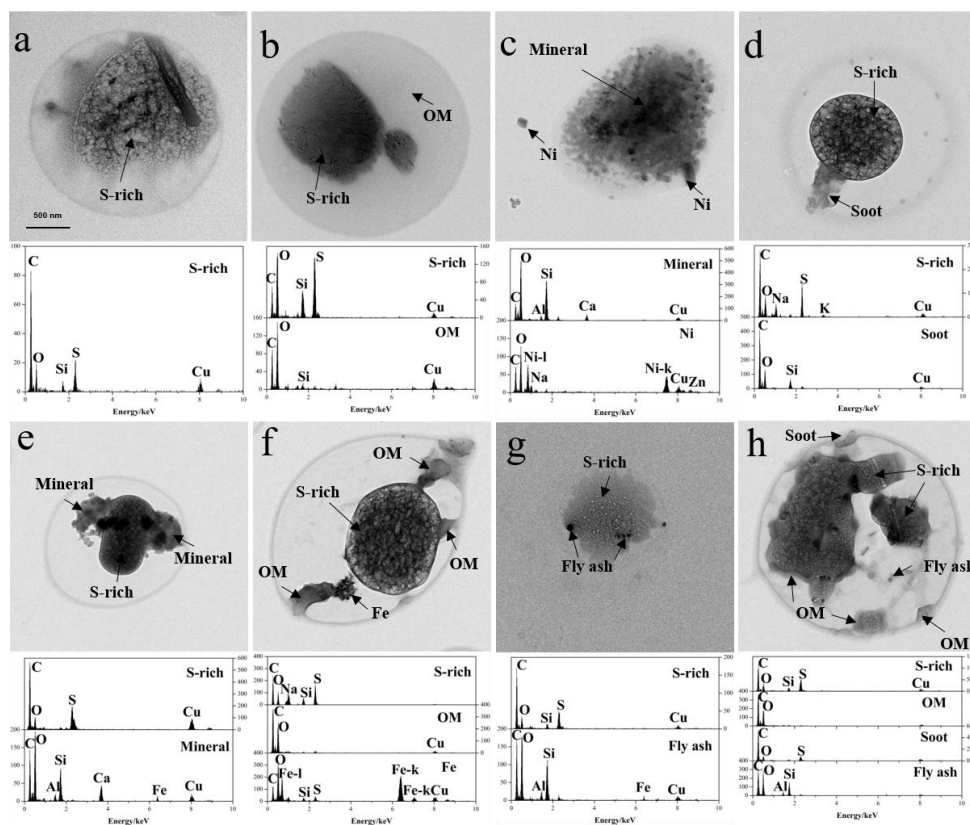
- 445 Ogawa, S., Setoguchi, Y., Kawana, K., Nakayama, T., Ikeda, Y., Sawada, Y., Matsumi, Y., and Mochida, M.:
446 Hygroscopicity of aerosol particles and CCN activity of nearly hydrophobic particles in the urban atmosphere
447 over Japan during summer, *Journal of Geophysical Research-Atmospheres*, 121, 7215-7234,
448 10.1002/2015jd024636, 2016.
- 449 Ovadnevaite, J., Zuend, A., Laaksonen, A., Sanchez, K. J., Roberts, G., Ceburnis, D., Decesari, S., Rinaldi, M.,
450 Hodas, N., Facchini, M. C., Seinfeld, J. H., and Dowd, C. O.: Surface tension prevails over solute effect in
451 organic-influenced cloud droplet activation, *Nature*, 546, 637-641, 10.1038/nature22806, 2017.
- 452 Petters, M. D., and Kreidenweis, S. M.: A single parameter representation of hygroscopic growth and cloud
453 condensation nucleus activity, *Atmospheric Chemistry and Physics*, 7, 1961-1971, 10.5194/acp-7-1961-2007,
454 2007.
- 455 Pierce, J. R., Leaitch, W. R., Liggio, J., Westervelt, D. M., Wainwright, C. D., Abbatt, J. P. D., Ahlm, L., Al-
456 Basheer, W., Cziczo, D. J., Hayden, K. L., Lee, A. K. Y., Li, S. M., Russell, L. M., Sjostedt, S. J., Strawbridge,
457 K. B., Travis, M., Vlasenko, A., Wentzell, J. J. B., Wiebe, H. A., Wong, J. P. S., and Macdonald, A. M.:
458 Nucleation and condensational growth to CCN sizes during a sustained pristine biogenic SOA event in a
459 forested mountain valley, *Atmospheric Chemistry and Physics*, 12, 3147-3163, 10.5194/acp-12-3147-2012,
460 2012.
- 461 Qiu, C., Khalizov, A. F., and Zhang, R.: Soot Aging from OH-Initiated Oxidation of Toluene, *Environmental*
462 *Science & Technology*, 46, 9464-9472, 10.1021/es301883y, 2012.
- 463 Radney, J. G., You, R., Ma, X., Conny, J. M., Zachariah, M. R., Hodges, J. T., and Zangmeister, C. D.:
464 Dependence of Soot Optical Properties on Particle Morphology: Measurements and Model Comparisons,
465 *Environmental Science & Technology*, 48, 3169-3176, 10.1021/es4041804, 2014.
- 466 Raymond, T. M., and Pandis, S. N.: Cloud activation of single-component organic aerosol particles, *Journal of*
467 *Geophysical Research-Atmospheres*, 107, D24, 10.1029/2002jd002159, 2002.
- 468 Riva, M., Chen, Y., Zhang, Y., Lei, Z., Olson, N. E., Boyer, H. C., Narayan, S., Yee, L. D., Green, H. S., Cui, T.,
469 Zhang, Z., Baumann, K., Fort, M., Edgerton, E., Budisulistiorini, S. H., Rose, C. A., Ribeiro, I. O., e Oliveira,
470 R. L., dos Santos, E. O., Machado, C. M. D., Szopa, S., Zhao, Y., Alves, E. G., de Sá, S. S., Hu, W., Knipping,
471 E. M., Shaw, S. L., Duvoisin Junior, S., de Souza, R. A. F., Palm, B. B., Jimenez, J.-L., Glasius, M., Goldstein,
472 A. H., Pye, H. O. T., Gold, A., Turpin, B. J., Vizuete, W., Martin, S. T., Thornton, J. A., Dutcher, C. S., Ault,
473 A. P., and Surratt, J. D.: Increasing Isoprene Epoxydiol-to-Inorganic Sulfate Aerosol Ratio Results in Extensive
474 Conversion of Inorganic Sulfate to Organosulfur Forms: Implications for Aerosol Physicochemical Properties,
475 *Environmental Science & Technology*, 53, 8682-8694, doi:10.1021/acs.est.9b01019, 2019.
- 476 Roth, A., Schneider, J., Klimach, T., Mertes, S., van Pinxteren, D., Herrmann, H., and Borrmann, S.: Aerosol
477 properties, source identification, and cloud processing in orographic clouds measured by single particle mass
478 spectrometry on a central European mountain site during HCCT-2010, *Atmospheric Chemistry and Physics*,
479 16, 505-524, 10.5194/acp-16-505-2016, 2016.
- 480 Scott, C. E., Rap, A., Spracklen, D. V., Forster, P. M., Carslaw, K. S., Mann, G. W., Pringle, K. J., Kivekäs, N.,
481 Kulmala, M., Lihavainen, H., and Tunved, P.: The direct and indirect radiative effects of biogenic secondary
482 organic aerosol, *Atmospheric Chemistry and Physics*, 14, 447-470, 10.5194/acp-14-447-2014, 2014.



- 483 Shingler, T., Dey, S., Sorooshian, A., Brechtel, F. J., Wang, Z., Metcalf, A., Coggon, M., Mülmenstädt, J., Russell,
484 L. M., Jonsson, H. H., and Seinfeld, J. H.: Characterisation and airborne deployment of a new counterflow
485 virtual impactor inlet, *Atmospheric Measurement Techniques*, 5, 1259-1269, 10.5194/amt-5-1259-2012, 2012.
- 486 Shiraiwa, M., Zuend, A., Bertram, A. K., and Seinfeld, J. H.: Gas-particle partitioning of atmospheric aerosols:
487 interplay of physical state, non-ideal mixing and morphology, *Physical Chemistry Chemical Physics*, 15,
488 11441-11453, 10.1039/c3cp51595h, 2013.
- 489 Song, M., Marcolli, C., Krieger, U. K., Lienhard, D. M., and Peter, T.: Morphologies of mixed
490 organic/inorganic/aqueous aerosol droplets, *Faraday Discussions*, 165, 289-316, 10.1039/c3fd00049d, 2013.
- 491 Spracklen, D. V., Jimenez, J. L., Carslaw, K. S., Worsnop, D. R., Evans, M. J., Mann, G. W., Zhang, Q.,
492 Canagaratna, M. R., Allan, J., Coe, H., McFiggans, G., Rap, A., and Forster, P.: Aerosol mass spectrometer
493 constraint on the global secondary organic aerosol budget, *Atmospheric Chemistry and Physics*, 11, 12109-
494 12136, 10.5194/acp-11-12109-2011, 2011.
- 495 Topping, D. O., McFiggans, G. B., Kiss, G., Varga, Z., Facchini, M. C., Decesari, S., and Mircea, M.: Surface
496 tensions of multi-component mixed inorganic/organic aqueous systems of atmospheric significance:
497 measurements, model predictions and importance for cloud activation predictions, *Atmospheric Chemistry and
498 Physics*, 7, 2371-2398, 10.5194/acp-7-2371-2007, 2007.
- 499 Wang, Y., Liu, F., He, C., Bi, L., Cheng, T., Wang, Z., Zhang, H., Zhang, X., Shi, Z., and Li, W.: Fractal
500 Dimensions and Mixing Structures of Soot Particles during Atmospheric Processing, *Environmental Science
501 & Technology Letters*, 4, 487-493, 10.1021/acs.estlett.7b00418, 2017.
- 502 Wu, Y., Cheng, T., Liu, D., Allan, J. D., Zheng, L., and Chen, H.: Light Absorption Enhancement of Black Carbon
503 Aerosol Constrained by Particle Morphology, *Environmental Science & Technology*, 52, 6912-6919,
504 10.1021/acs.est.8b00636, 2018.
- 505 Wu, Z. J., Poulain, L., Henning, S., Dieckmann, K., Birmili, W., Merkel, M., van Pinxteren, D., Spindler, G.,
506 Mueller, K., Stratmann, F., Herrmann, H., and Wiedensohler, A.: Relating particle hygroscopicity and CCN
507 activity to chemical composition during the HCCT-2010 field campaign, *Atmospheric Chemistry and Physics*,
508 13, 7983-7996, 10.5194/acp-13-7983-2013, 2013.
- 509 Yu, H., Li, W., Zhang, Y., Tunved, P., Dall'Osto, M., Shen, X., Sun, J., Zhang, X., Zhang, J., and Shi, Z.: Organic
510 coating on sulfate and soot particles during late summer in the Svalbard Archipelago, *Atmospheric Chemistry
511 and Physics*, 19, 10433-10446, 10.5194/acp-19-10433-2019, 2019.
- 512 Yuan, Q., Xu, J., Wang, Y., Zhang, X., Pang, Y., Liu, L., Bi, L., Kang, S., and Li, W.: Mixing State and Fractal
513 Dimension of Soot Particles at a Remote Site in the Southeastern Tibetan Plateau, *Environmental Science &
514 Technology*, 53, 8227-8234, 10.1021/acs.est.9b01917, 2019.
- 515 Zelenyuk, A., Imre, D., Earle, M., Easter, R., Korolev, A., Leaitch, R., Liu, P., Macdonald, A. M., Ovchinnikov,
516 M., and Strapp, W.: In Situ Characterization of Cloud Condensation Nuclei, Interstitial, and Background
517 Particles Using the Single Particle Mass Spectrometer, SPLAT II, *Analytical Chemistry*, 82, 7943-7951,
518 10.1021/ac1013892, 2010.
- 519 Zhang, G., Lin, Q., Peng, L., Bi, X., Chen, D., Li, M., Li, L., Brechtel, F. J., Chen, J., Yan, W., Wang, X., Peng,
520 P., Sheng, G., and Zhou, Z.: The single-particle mixing state and cloud scavenging of black carbon: a case study
521 at a high-altitude mountain site in southern China, *Atmospheric Chemistry and Physics*, 17, 14975-14985,
522 10.5194/acp-17-14975-2017, 2017a.

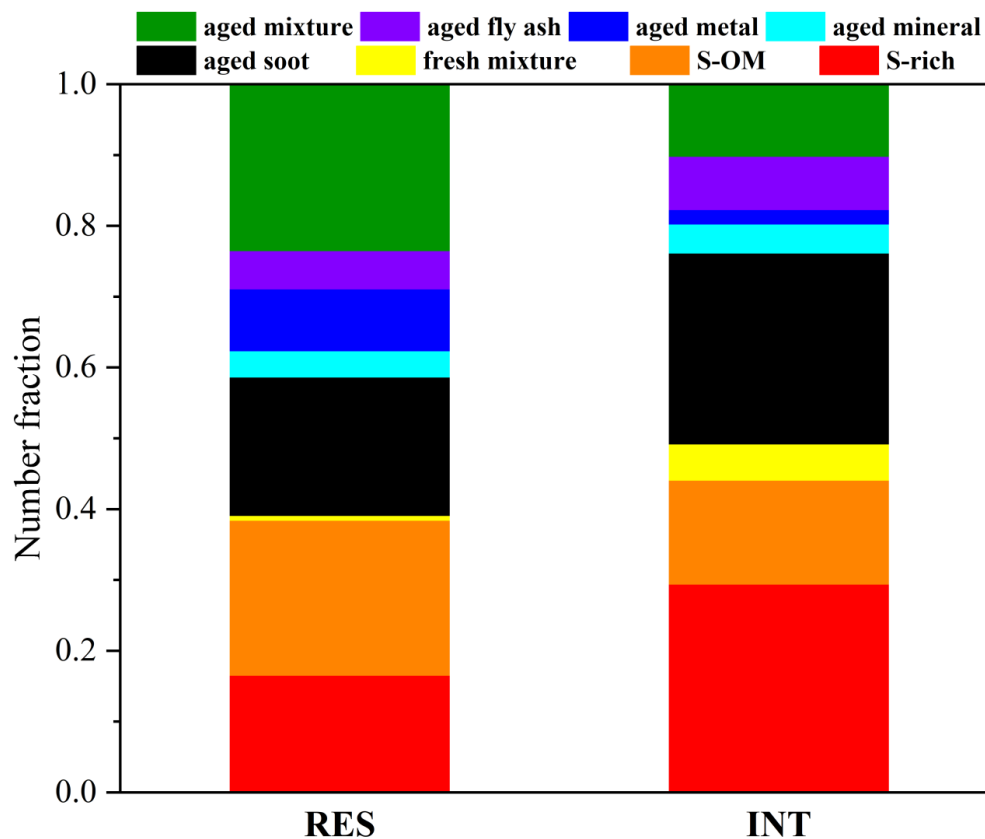


- 523 Zhang, G., Lin, Q., Peng, L., Yang, Y., Fu, Y., Bi, X., Li, M., Chen, D., Chen, J., Cai, Z., Wang, X., Peng, P.,
524 Sheng, G., and Zhou, Z.: Insight into the in-cloud formation of oxalate based on in situ measurement by single
525 particle mass spectrometry, *Atmospheric Chemistry and Physics*, 17, 13891-13901, 10.5194/acp-17-13891-
526 2017, 2017b.
- 527 Zhang, Y., Chen, Y., Lambe, A. T., Olson, N. E., Lei, Z., Craig, R. L., Zhang, Z., Gold, A., Onasch, T. B., Jayne,
528 J. T., Worsnop, D. R., Gaston, C. J., Thornton, J. A., Vizuete, W., Ault, A. P., and Surratt, J. D.: Effect of the
529 Aerosol-Phase State on Secondary Organic Aerosol Formation from the Reactive Uptake of Isoprene-Derived
530 Epoxydiols (IEPOX), *Environmental Science & Technology Letter*, 5, 167-174,
531 doi:10.1021/acs.estlett.8b00044, 2018.
- 532 Zhang, Y., Chen, Y., Lei, Z., Olson, N. E., Riva, M., Koss, A. R., Zhang, Z., Gold, A., Jayne, J. T., Worsnop, D.
533 R., Onasch, T. B., Kroll, J. H., Turpin, B. J., Ault, A. P., and Surratt, J. D.: Joint Impacts of Acidity and Viscosity
534 on the Formation of Secondary Organic Aerosol from Isoprene Epoxydiols (IEPOX) in Phase Separated
535 Particles, *ACS Earth Space Chem.*, 3, 2646-2658, doi:10.1021/acsearthspacechem.9b00209, 2019.
- 536 Zhang, Y., Yuan, Q., Huang, D., Kong, S., Zhang, J., Wang, X., Lu, C., Shi, Z., Zhang, X., Sun, Y., Wang, Z.,
537 Shao, L., Zhu, J., and Li, W.: Direct Observations of Fine Primary Particles From Residential Coal Burning:
538 Insights Into Their Morphology, Composition, and Hygroscopicity, *Journal of Geophysical Research-
539 Atmospheres*, 123, 12964-12979, 10.1029/2018jd028988, 2018.
- 540 Zhu, J., Penner, J. E., Lin, G., Zhou, C., Xu, L., and Zhuang, B.: Mechanism of SOA formation determines
541 magnitude of radiative effects, *Proceedings of the National Academy of Sciences of the United States of
542 America*, 114, 12685-12690, 10.1073/pnas.1712273114, 2017.



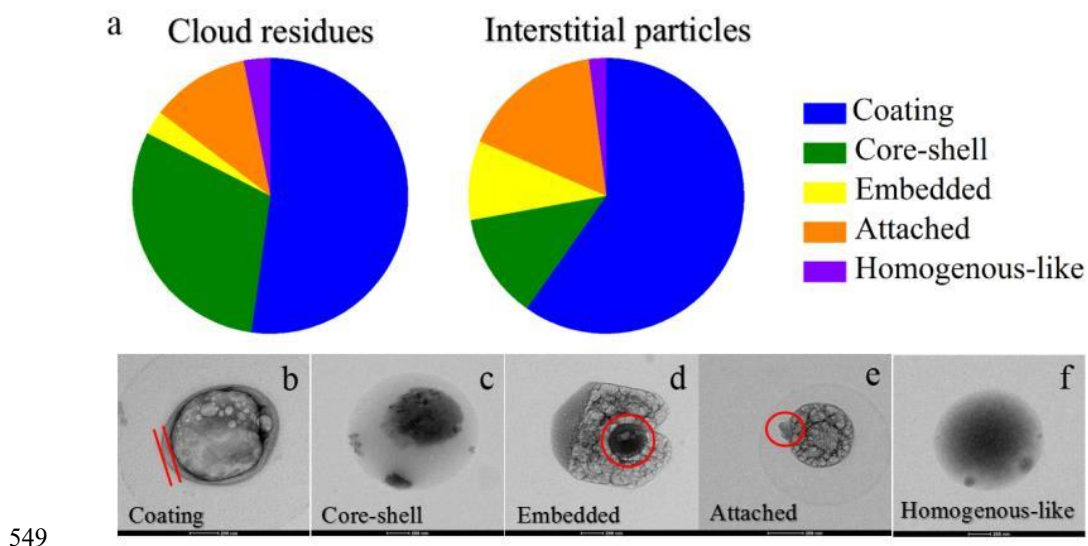
543

544 Figure 1. TEM images and EDS spectra of individual RES and INT particles with different particle types: (a) S-rich;
545 (b) S-OM; (c) fresh mixture; (d) aged soot; (e) aged mineral; (f) aged metal; (g) aged fly ash; (h) aged mixture.

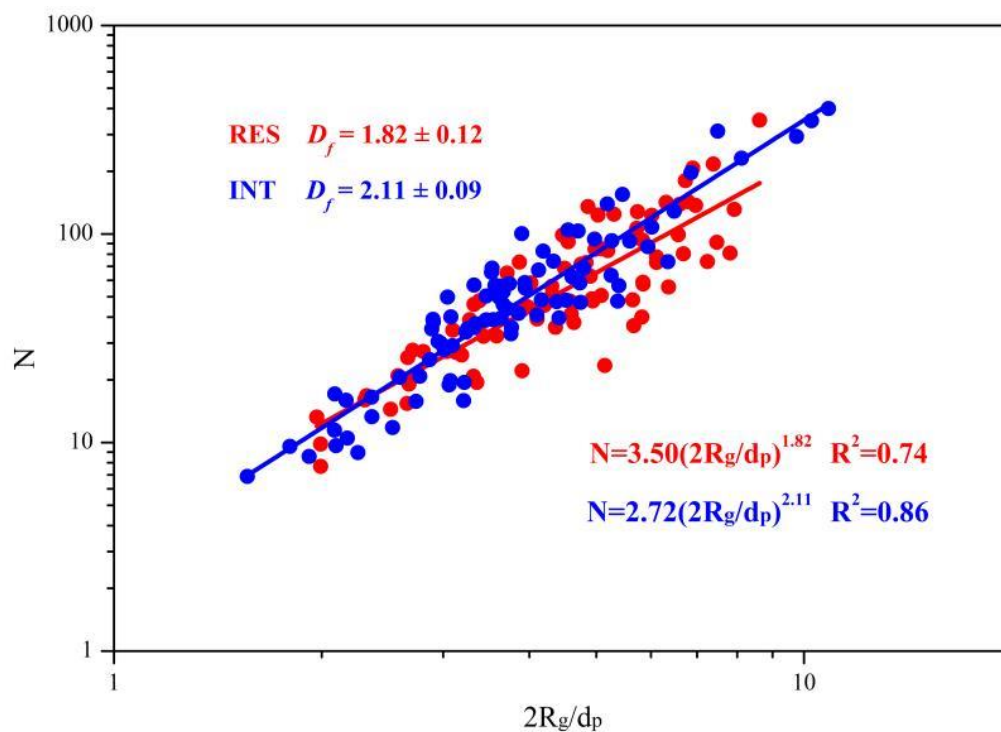


546

547 Figure 2. Number fractions of different particle types in the RES and INT of cloud event #2 and #3 measured by
548 TEM/EDS.



550 Figure 3. Number fractions of OM-containing particles with different mixing structures in the RES and INT (a) and
551 typical TEM images: coating (b); core-shell (c); embedded (d); attached (e); homogenous-like (f) during cloud event #2
552 and #3.



553

554 Figure 4. Fractal dimensions of soot in the RES and INT during cloud event #2 and #3.